Computer Assisted Mechanics and Engineering Sciences, 14: 405–429, 2007.

Application of elasto-viscoplastic Bodner–Partom constitutive equations in finite element analysis

Andrzej Ambroziak
Gdańsk University of Technology, Faculty of Civil and Environmental Engineering
Department of Structural Mechanics and Bridge Structures,
Narutowicza 11/12, 80-952 Gdańsk

(Received June 10, 2005)

A finite element implementation of the unified elasto-viscoplastic theory of Bodner–Partom for non-linear analysis is investigated in detail. Description of the Bodner–Partom constitutive equations is presented. Proposed UVSCPL procedure has been applied into MSC.Marc system and can be introduced into wide range of different finite elements (e.g. shell, solid, truss). For the validation of the proposed FE procedure the numerical simulations are presented. Additionally, the first part of the paper gives brief characterization of the engineering applications of the Bodner–Partom constitutive equations used for the different modelling of materials.

Keywords: elasto-viscoplastic constitutive model, Bodner–Partom, FEM

1. Introduction

Rate-dependent plasticity and creep are major concerns in the structural analysis of the materials beyond the yield limit or subjected to cyclic loading under different temperatures. In recent years, a large number of constitutive equations has been proposed for the description of the elasto-viscoplastic material behaviour. Among others it is possible to specify the following models proposed by: Perzyna [53], Bodner–Partom [11], Miller [48], Tanimura [67], Krempl [40], Lehmann–Imatani [43], Chaboche [14], Krieg–Swearengen–Jones [41], Korhonen–Hannula–Le [39], Freed–Verrilli [22], Walker [23], Aubertin [6]. The practical engineering applications of the models specified above are limited due to difficulties with identification of large number of material constants.

In these enumerated models, all mechanisms of the inelastic effects are represented by a single kinetic equation that defines the inelastic strain rate $\dot{\varepsilon}^I$. Additionally, all of them are based on the assumption of the strain additivity,

$$\dot{\varepsilon} = \dot{\varepsilon}^E + \dot{\varepsilon}^I, \tag{1}$$

where $\dot{\varepsilon}$, $\dot{\varepsilon}^E$ and $\dot{\varepsilon}^I$ are total strain rate, elastic part of the total strain rate and inelastic part of the total strain rate, respectively.

In the present paper the author makes the detailed investigation for the Bodner–Partom elasto-viscoplastic model. In the first part of the paper the literature survey of the numerical, scientific and engineering applications is given. The second part gives the examples of the static and dynamic finite element analysis.

2. Applications review of the Bodner–Partom model

The unified plasticity approach is based on the use of a single variable that represents all the inelastic deformations and can be developed in formulations with or without a yield criterion. An objective of a unified constitutive theory is that it can be applicable for some classes of materials over a wide range of strain rates and temperatures. The Bodner–Partom constitutive model was one of the unified theories proposed by Bodner and Partom [11] in the 1970s. The Bodner–Partom constitutive equations have been frequently utilized for modelling the elasto-viscoplastic hardening of number materials. This model is used in many practical engineering applications, which are presented in this section in the compact form.

Rubin [54] developed a unconditionally stable numerical procedure for time integration of the flow rule for large plastic deformation of an metal. He focused specific attention on unified Bodner–Partom constitutive equations. Numerical examples of simple shear, a corner test exhibiting the transition from uniaxial compression to shear, and simple tension are considered which demonstrate the stability and accuracy of the procedure.

Sung and Achenbach [66] studied a crack propagating in a viscoplastic material with the Bodner–Partom model. On the basis of the adiabatic approximation, the maximum temperature is investigated as a function of the crack-tip velocity and the material parameters. Assuming small strains and moderate rotations Kłosowski *et al.* [33] investigated the elasto-viscoplastic dynamic behaviour of plates and shells. The Chaboche [14] and Bodner–Partom [12] models were chosen by the authors to the description of the steel material behaviour. To avoid the calculation of the stiffness matrix, an effective procedure using the central difference method of solving the equations of motion was applied. A nine-node isoparametric shell element was utilised for the finite element algorithm.

The kinematic quantities needed for the description of finite deformations with inelastic constitutive models and the formulation of an inelastic material model for large deformations are summarized by Hackenberg [25]. The extended Bodner–Partom model, which includes damage effects (based on Gurson's model) was described. An approximation of the constitutive model is given which takes into account the volumetric constraint and which is suitable for the incremental numerical scheme. The elasto-viscoplastic equations of Bodner–Partom was modified to model strong non-proportional loading path such as experienced in corner turning tests and certain cases of inelastic buckling by Rubin and Bodner [55]. An essential generalization is made to the flow rule, causing the magnitude and direction of plastic strain rate to become an explicit function of deviatoric total strain rate as well as of stress and hardening variables.

A numerical method for the implementation of a micromechanical model capable of predicting the thermomechanical response of laminated metal matrix composites in the presence of damage development with the Bodner–Partom model was developed by Lissenden and Herakovich [46]. The non-linear lamination theory used by the authors provided the link between the micro- and macro-level responses of laminated composites subjected to thermomechanical loading. In the work [47] Mahnken and Stein presented a unified strategy for identification of material parameters of Chaboche [14], Bodner–Partom [11] and Steck [63] viscoplastic constitutive models from uniaxial tests. The gradient-based descent methods for minimization of a least squares functional, thus requiring the associative gradient was used. The numerical examples in the context of monotonic and cyclic loading were described too.

Arya [5] developed a explicit integration algorithms with self-adaptive time integration strategies which are applied to numerical analysis with Bodner–Partom and Freed–Verrilli [22] models. The large amount of computations performed showed that the efficiency of an integration algorithm depends significantly on the type of application. To the description of behaviour of the high-density polyethylene Zhang and Moore [77] used the Bodner–Partom and the extended Kelvin models. Based on the uniaxial tension tests the material parameters for both models were established. Limitations in the application of each model were discussed too.

Foringer *et al.* [20] described fatigue life modelling of titanium-based MMCs (metal-matrix composites). In this paper two composites SCS-6/Timetal21s and SCS-6/Ti-15-3 were investigated.

For the modelling the authors have used the Bodner–Partom constitutive model with non-linear micromechanics analysis and damage accumulation model. An evolution equations of the Bodner–Partom type with the concept of the multiplicative decomposition of the deformation gradient are employed with different numerical examples of finite strain deformations by Sansour and Kollmann [57]. Kroupa and Bartsch [42] investigated an improved formulation for the viscoplastic response of Timetalt21S matrix. Modifications to the Bodner–Partom constitutive equations provide improved flexibility in fitting a larger strain-rate range than previously available.

The material parameters of the isotropic form of the Bodner–Partom model were found for the eutectic solder as functions of temperature by Skipor and Harren [61]. The resulting temperature dependent viscoplastic description for the eutectic is implemented in an infinitesimal strain incrementally linear finite element method (FEM). The results of the analyses show that, along with observed field performance of solder joints, the details of the plastic strain distribution within a joint can have large impact on joint reliability. Sansour and Kollmann [56] studied the large inelastic deformations of shells when the constitutive model is based on the concept of unified Bodner–Partom evolution constitutive equations. An algorithm for the evaluation of the exponential map for non-symmetric arguments as well as a closed form of the tangent operator were given. An enhanced strain FEM was given and various examples of large shell deformations including loading–unloading cycles were presented. The constitutive models for metals: Johnson–Cook [29], Zerilli–Armstrong [76], Bodner–Partom and Khan–Huang [30] were investigated by Liang and Khan [45] and have been used to predict the mechanical behaviours of metals. Limitations for each model in describing work-hardening behaviour of metals were discussed.

An implementation of the unified theory of Bodner–Partom in a three-dimensional finite element program for the analysis of anisotropic inelastic metals behaviour were given by Esat *et al.* [19]. A comparison of the results of the finite element analysis with experimental results for pure titanium and 2024-T4 aluminium alloy was presented in details. Kłosowski *et al.* [36] studied vibrations of the circular plates subjected to shock-wave impulses. In this paper two constitutive equations types of the Chaboche and Bodner–Partom models were used to the description of the elasto-viscoplastic plates behaviour. Results of a finite element analysis (FEA) were compared with experimental data. Woznica and Kłosowski [72] proposed identification method to determine the material parameters for Bodner–Partom and Chaboche constitutive models using tensile tests. Chełmiński [16] studied existence and the uniqueness of global in time, strong, large solutions to the inelastic model of Bodner–Partom with non-homogeneous boundary conditions with the perturbation term in the equation for the isotropic hardening function. An axisymmetric dynamic thermo-viscoelastic problem was formulated with allowance for the coupling of mechanical and thermal fields by Zhuk *et al.* [78]. The behaviour of the material was described by the Bodner–Partom model. A technique for numerical solution of the problem was developed. The laws governing the stress–strain state and the temperature field of a circular disk under forced flexural vibrations were studied.

Barta and Jaber [8] used the Litonski–Batra, Johnson–Cook, Bodner–Partom and the power law thermoviscoplastic constitutive relations to model the thermoviscoplastic response of a material. The material parameters in these relations were found by solving an initial-boundary-value problem corresponding to simple shearing deformations with the experimental data of thin-walled HY-100 steel tubes in torsion. These four viscoplastic relations were used to analyze dynamic thermo-mechanical deformations of a prenotched plate impacted on the notched side by a cylindrical projectile made of the same material as the plate. The fibber-matrix interactions and effective elasto-plastic properties of aligned short-fibber-reinforced metal matrix composite was studied by Yang and Qin [73] by using a micromechanical model and FEA. The fibber was assumed to be elastic and the matrix to be elasto-viscoplastic continuum described by B-P unified theory of plasticity. The local elasto-plastic stress fields of a unit cell in composite were examined in order to understand the mechanism of inelastic deformations and interactions between fibbers and matrix. The authors predicted elasto-viscoplastic properties of B/Al composites by the domain average method. Application of the Bodner–Partom constitutive equations for glassy polymers were described by Frank and Brockman [21]. The model was implemented into a FEA program and appropriate parameters were identified for a polycar-

bonate. Capabilities of the model were demonstrated through the evolution of hard-body impact problem. Gwizda [24] investigated the global in time existence of large solutions for a problem in non-linear inelastic with viscosity. In this paper the Bodner–Partom model was studied in details. The proofs were based on the energy methods.

The wall ironing process of sheet metal coated with a polymer layers was investigated by Aa *et al.* [70]. It should be noted that the material behaviour of metal sheet was specified by Bodner–Partom model while the polymer layers by the Leonov model [44]. Sansour and Wagner [58, 59] presented a framework of additive models of finite strain plasticity and viscoplasticity. The Bodner–Partom evolution equations have been modified so as to fit into the theoretical framework adopted. The numerical treatment of the problem was fully developed. Specifically, the algorithmic aspects of the approach were discussed and various applications to shell problems were considered. Crack growth tests on specimens with rectangular cross-section of Incotel 718°C at 550 and 627°C in order to examine the low-cycle fatigue behaviour were investigated by Andersson *et al.* [4]. The material was described in terms of the Bodner–Partom viscoplastic constitutive equations. The material parameters were found by fitting simulations to the experimental data. The Bodner–Partom equations were implemented in Matlab and were used to estimate the stress response for the strain history. A FE implementation of the unified elasto-viscoplastic theory of Bodner for the analysis of metal matrix composites was presented by Shati *et al.* [60]. An original model of circular fibres embedded in a square array of matrix material was chosen. The results of the analysis for two aluminium matrix composites were compared with the results of Aboudi's continuum theory and the Halpin–Tsai equations. Barta and Chen [7] studied the thermomechanical steel block deformations deformed in simple shear. To the description of the material behaviour a four different constitutive equations: the Wright–Batra, Johnson–Cook, power law and the Bodner–Partom were used. The authors have used the perturbation method to analyze the stability of a homogeneous solution of the governing equations.

Bodner [13] introduced the unified theories of elasto-viscoelastic material behaviour combining all aspects of inelastic responses into a set of time-dependent equations with a single inelastic strain rate variable. In this monograph, the first section contains a formulation of a unified constitutive theory for elastic-viscoplastic behaviour. Special attention is given to the representation of material behaviour at high and very high strain rates. The third section of the monograph discusses the status of the unified theory of Bodner and Partom and some further developments for large deformations and finishes with a computer programme for uniaxial stress and isotropic and directional hardening. The framework for an implicit implementation of the Bodner–Partom material model was presented by Anderson [3]. The author derived equations needed for using a Newton–Raphson algorithm to solve the stress and hardening equations. Song *et al.* [62] presented the application of Bodner–Partom model in FEA of high velocity impact. The material parameters were determined on the basis of the experiments of Hopkins bar tests. A detailed description of the split Hopkinson pressure bar technique is given e.g. by Klepaczko [31]. The impact process runs in so quick time that the heat-conducting can be neglected. Therefore the functions of temperature in equations need to be replaced by functions of plastic work.

Batra *et al.* [9] numerically investigated the effect on the failure mode transition speed of the shape of the notch-tip and the presence of a hole ahead of a circular notch-tip. The Bodner–Partom thermoviscoplastic relation was used to model the strain hardening, strain-rate hardening and thermal softening response of the material of the plate. The transient plane strain thermomechanical deformations of the plate were analyzed by the finite element method. The effects of the shape of the notch-tip and of the presence of a circular hole located ahead of the circular notch-tip on the initiation of a failure mode were scrutinized. The Bodner–Partom constitutive model was developed for predicting the thermal and mechanical responses of a cobalt-based ULTIMET alloy subjected to cyclic deformation by Jiang *et al.* [28]. The model was constructed in light of internal state variables, which were developed to characterize the inelastic strain of the material during cyclic loading. The predicted stress–strain and temperature responses were found to be in good agreement with the experimental results.

The influence of higher order terms which should be taken into account in the strain-displacement relations for shell according to moderate or large rotations theories were detailed studied by Kłosowski and Woznica [35]. The different types of the viscoplastic constitutive models (Perzyna [52], Chaboche, Bodner–Partom) applied for FE problems were investigated. Hart *et al.* [26] introduced stochastic methods to describe the influence of scattering test data on the identification of material parameters for Bodner–Partom model. The material parameters were determined for AINSI SS316 stainless steel at 600°C on the basis of creep tests, constant strain rate tension tests and cyclic tension-compression tests. Kłosowski *et al.* [37] described the results of the technical Panama fabric experiments with the purpose of identification of inelastic properties of the warp and weft. The Bodner–Partom and Chaboche viscoplastic models were applied to the description of the warp and weft properties. The material parameters were calculated on the basis of the uniaxial tension test in the warp and weft directions. The results are verified by numerical simulation of the laboratory tests. Stoffel [65] in order to predict the inelastic deformations of shock wave loaded plates simulations used viscoplastic constitutive equations of Chaboche and Bodner–Partom combined with a structural theory.

Application of the unified elastic-viscoplastic Bodner–Partom model to the description of the nonlinear behaviour of glass polymers was investigated by Zaïri *et al.* [75]. To represent the nonlinear behaviour and the effect of rate, a single rate independent set parameters is determined from an original procedure. The modified Bodner–Partom model associated with the original version shown sufficient flexibility to permit modelling of the representative amorphous glassy polymer response. Uniaxial tension tests on a RT-PMMA material by Zaïri *et al.* [74] were achieved under various constant strain rates. The experimental results revealed the presence of both the nucleation and growth deformation mechanisms. Modified viscoplastic constitutive equations for homogeneous glassy polymers at isothermal loading, including strain softening and strain hardening, was proposed. The modified Bodner–Partom model was coupled with a micromechanics formulation, using the Gurson–Tvergaard model, to investigate the macroscopic mechanical response of the RT-PMMA.

The author is aware that the applications of the Bodner–Partom model are widely discussed in the literature (short review is given above), but very often presented results of analyses and investigations are incomplete or difficult to obtain (technical reports).

3. Elasto-viscoplastic Bodner–Partom constitutive equations

In general, the strain rate $\dot{\boldsymbol{\sigma}}$ is specified by the time derivative of Hooke's law as

$$\dot{\boldsymbol{\sigma}} = \mathbf{D} : \dot{\boldsymbol{\varepsilon}}^E = \mathbf{D} : \left(\dot{\boldsymbol{\varepsilon}} - \dot{\boldsymbol{\varepsilon}}^I\right), \tag{2}$$

where $\mathbf{D}$ is the tensor of elastic modules. The stress in numerical calculation at the time t can be calculated as

$${}^{t}\boldsymbol{\sigma} = {}^{t-\Delta t}\boldsymbol{\sigma} + \Delta\boldsymbol{\sigma}, \tag{3}$$

where the stress increment $\Delta\boldsymbol{\sigma}$ is expressed as

$$\Delta\boldsymbol{\sigma} = \mathbf{D} : \Delta\boldsymbol{\varepsilon}^E = \mathbf{D} : \left(\Delta\boldsymbol{\varepsilon} - \Delta\boldsymbol{\varepsilon}^I\right), \tag{4}$$

while the inelastic strain increment $\Delta\boldsymbol{\varepsilon}^I$ can be calculated from the trapezoidal formula

$$\Delta\boldsymbol{\varepsilon}^I = \frac{{}^{t}\dot{\boldsymbol{\varepsilon}}^I + {}^{t+\Delta t}\dot{\boldsymbol{\varepsilon}}^I}{2} \cdot \Delta t, \tag{5}$$

or by using simple equation

$$\Delta\boldsymbol{\varepsilon}^I = {}^{t}\dot{\boldsymbol{\varepsilon}}^I \cdot \Delta t. \tag{6}$$

In the Bodner–Partom model the inelastic strain rate $\dot{\varepsilon}^I$ is given by the equation

$$\dot{\varepsilon}^I = \frac{3}{2} \cdot \dot{p} \cdot \frac{\sigma'}{J(\sigma')}, \tag{7}$$

where $\dot{p}$, σ' and $J(\sigma')$ are the equivalent plastic strain, the deviatoric parts of stress and the stress invariant, respectively. It should be noted that in the model it is assumed the existence of the inelastic deformation from the very beginning of the deformation process. The invariant $J(\sigma')$ may be expressed directly in terms of the deviatoric parts of stress σ' by the formula

$$J(\sigma') = \sqrt{\frac{3}{2}(\sigma' : \sigma')}. \tag{8}$$

The rate of the equivalent plastic strain $\dot{p}$ is defined by (see e.g. Bodner and Partom [11])

$$\dot{p} = \frac{2}{\sqrt{3}} \cdot D_0 \cdot \exp\left[-\frac{1}{2} \cdot \left(\frac{R+D}{J(\sigma')}\right)^{2 \cdot n} \cdot \frac{n+1}{n}\right]. \tag{9}$$

where

$$D = \mathbf{X} : \frac{\sigma}{J(\sigma)}. \tag{10}$$

The material parameters D_0 and n represent the limiting plastic strain rate and the strain rate sensitivity parameter. In this model it is assumed that the variable D_0 is fixed for a strain range. In [49], Bodner recommended the following values for the maximum value of D_0 (see Table 1).

Table 1. Values for D_0 parameter

$\dot{\varepsilon}^I$ [s^{-1}]	< 10	$10 \div 10^3$	$> 10^3$
D_0 [s^{-1}]	10^4	10^6	10^7

In the literature, it is possible to find another form (see e.g. Chan *et al.* [15]) of the rate of the equivalent strain rate $\dot{p}$ given by

$$\dot{p} = \frac{2}{\sqrt{3}} \cdot D_0 \cdot \exp\left[-\frac{1}{2} \cdot \left(\frac{R+D}{J(\sigma')}\right)^{2 \cdot n}\right]. \tag{11}$$

The evolution of isotropic hardening R is defined as

$$\dot{R} = m_1 \cdot (Z_1 - R) \cdot (\sigma : \dot{\varepsilon}^I) - A_1 \cdot Z_1 \cdot \left(\frac{R - Z_2}{Z_1}\right)^{r_1}, \tag{12}$$

where m_1, A_1, r_1, Z_1 and Z_2 are the hardening rate coefficient, recovery coefficient, recovery exponent, limiting (maximum) value and fully recovered (minimum) value for isotropic hardening, respectively. Additionally, at the beginning of calculation the isotropic hardening has the initial value Z_0, thus $R(t{=}0) = Z_0$.

The evolution of kinematic hardening $\mathbf{X}$ is expressed by the equation

$$\dot{\mathbf{X}} = m_2 \cdot \left(\frac{3}{2} \cdot Z_3 \cdot \frac{\sigma}{J(\sigma)} - \mathbf{X}\right) \cdot (\sigma : \dot{\varepsilon}^I) - A_2 \cdot Z_1 \cdot \frac{3}{2} \cdot \left[\frac{\frac{2}{3} J(\mathbf{X})}{Z_1}\right]^{r_2} \cdot \frac{\mathbf{X}}{J(\mathbf{X})}, \tag{13}$$

where m_2, A_2, r_2 and Z_3 are the hardening rate coefficient, recovery coefficient, recovery exponent and limiting (maximum) value for kinematic hardening, respectively.

In this described model the 14 parameters have to be determined (E, ν, D_0, n, Z_0, m_1, Z_1, A_1, Z_2, r_1, m_2, Z_3, A_2, r_2). In [12] Bodner applied the reduced number of parameters making an assumption: $Z_2 = Z_0$, $A_1 = A_2 = A$ and $r_1 = r_2 = r$.

Bodner and Chan [10] described procedure for including isotropic and directional damage as load-history dependent softening variables. Directional damage is represented as the second-order symmetric tensor with a scalar effective value. In the case of the isotropic continuum damage development assumption, the damage expression D (suggested by Bodner and Chan [10]) can be described under multiaxial stress as

$$\dot{D} = \frac{h}{H} \cdot \left[\ln \left(\frac{1}{D} \right)^{\frac{h+1}{h}} \right] \cdot D \cdot \dot{Q}, \tag{14}$$

where h, H are damage material constants. The multiaxial stress function Q has the form (see Hayhurst [27] for details)

$$\dot{Q} = \left(\alpha_1 \cdot \sigma^{+}_{\max} + \alpha_2 \cdot J(\boldsymbol{\sigma}) + \alpha_3 \cdot \operatorname{tr} (\boldsymbol{\sigma})^{+} \right)^{z}, \tag{15}$$

where α_1, α_2, α_3, z are the material constants. The parameters α_1, α_2 and α_3 satisfy the relation

$$\alpha_1 + \alpha_2 + \alpha_3 = 1.0. \tag{16}$$

The expressions $\sigma^{+}_{\max}$ and $\operatorname{tr} (\boldsymbol{\sigma})^{+}$ are the maximum principal tensile stress and the first stress invariant.

For example, in the case of the constant stress conditions the damage evolution D can be integrated to (see Bodner and Chan [10])

$$D = \exp \left[- \left(\frac{H}{Q} \right)^{h} \right]. \tag{17}$$

The rate of the equivalent plastic strain $\dot{p}$, with isotropic damage evolution has the form

$$\dot{p} = \frac{2}{\sqrt{3}} \cdot D_0 \cdot \exp \left[-\frac{1}{2} \cdot \left(\frac{\left(R + \left(\mathbf{X} : \frac{\boldsymbol{\sigma}}{J(\boldsymbol{\sigma})} \right) \right) \cdot (1 - D)}{J(\boldsymbol{\sigma}')} \right)^{2 \cdot n} \cdot \frac{n+1}{n} \right]. \tag{18}$$

It should be noted that in the case of damage analysis, the stress rate $\dot{\boldsymbol{\sigma}}$ is given by

$$\dot{\boldsymbol{\sigma}} = (1 - D) \cdot \mathbf{D} : \dot{\boldsymbol{\varepsilon}}^{E} = (1 - D) \cdot \mathbf{D} : \left(\dot{\boldsymbol{\varepsilon}} - \dot{\boldsymbol{\varepsilon}}^{I} \right). \tag{19}$$

4. Numerical simulations and discussion

4.1. Description of applied program and proposed UVSCPL procedure

From wide range of available commercial programs to the numerical analysis the MSC.Marc system was applied. It is a multi-purpose, FEA program for advanced engineering simulations with the possibility of introducing user-subroutines. The standard MSC.Marc system does not support the Bodner–Partom material models. To apply the Bodner–Partom model to the MSC.Marc system the user-defined subroutines UVSCPL [69] is used, where the inelastic strain rate and the stress increments must be specified. The flow graph of the procedure is given in Fig. 1. The full version of the UVSCPL subroutine is presented in Table 4.

$$\left[\begin{array}{ll} \Delta\mathbf{X} = \frac{\Delta t}{2} \cdot \left(\dot{\mathbf{X}}_{j-1} + \dot{\mathbf{X}}_j\right), & \mathbf{X}_j = \mathbf{X}_{j-1} + \Delta\mathbf{X} \\ \Delta R = \frac{\Delta t}{2} \cdot \left(\dot{R}_{j-1} + \dot{R}_j\right), & R_j = R_{j-1} + \Delta R \end{array}\right]$$

$$\left[\boldsymbol{\sigma}'_j,\ J(\boldsymbol{\sigma}'_j),\ J(\boldsymbol{\sigma}_j),\ J(\mathbf{X}_j)\right]$$

$$\left[\dot{p}_j = \frac{2}{\sqrt{3}} \cdot D_0 \cdot \exp\left[-\frac{1}{2} \cdot \left(\frac{(R+D)}{J(\boldsymbol{\sigma}'_j)}\right)^{2 \cdot n} \cdot \frac{n+1}{n}\right]\right]$$

$$\left[\dot{\boldsymbol{\varepsilon}}^I_j = \frac{3}{2}\dot{p}_j \frac{\boldsymbol{\sigma}'_j}{J(\boldsymbol{\sigma}'_j)}\right]$$

$$\left[\dot{R}_j = m_1 \cdot (Z_1 - R_j) \cdot (\boldsymbol{\sigma}_j : \dot{\boldsymbol{\varepsilon}}^I_j) - A_1 \cdot Z_1 \cdot \left(\frac{R_j + Z_2}{Z_1}\right)^{r_1}\right]$$

$$\left[\dot{\mathbf{X}}_j = m_2 \cdot \left(\frac{3}{2} \cdot Z_3 \cdot \frac{\boldsymbol{\sigma}_j}{J(\boldsymbol{\sigma}_j)} - \mathbf{X}_j\right) \cdot (\boldsymbol{\sigma}_j : \dot{\boldsymbol{\varepsilon}}^I_j)_j - A_2 \cdot Z_1 \cdot \frac{3}{2} \cdot \left(\frac{\frac{2}{3}J(\mathbf{X}_j)}{Z_1}\right)^{r_2} \cdot \frac{\mathbf{X}_j}{J(\mathbf{X}_j)}\right]$$

$$\left[\Delta\boldsymbol{\varepsilon}^I_j = \dot{\boldsymbol{\varepsilon}}^I_j \cdot \Delta t_j\right]$$

$$\left[\Delta\boldsymbol{\sigma}_j = \mathbf{D} \cdot (\Delta\boldsymbol{\varepsilon}_j - \Delta\boldsymbol{\varepsilon}^I_j)\right]$$

Fig. 1. Flow graph of the UVSCPL subroutine

4.2. Example 1

In order to confirm the correctness of implementation of Bodner–Partom equations to the MSC.Marc system using the UVSCPL subroutine the numerical calculations were carried out for simple shell, solid and truss structures The geometry and boundary conditions of these structures were assumed in order to compare the obtained numerical results with the uniaxial tension tests. In the experiments, specimens of the steel metal sheet had the following dimensions: width $b = 12.5\,\text{mm}$, length $l = 70\,\text{mm}$ and thicknesses $t = 1\,\text{mm}$.

In the MSC.Marc calculations the four-node thin-shell (Element 139, [68]), the three-dimensional eight-node isoparametric solid (Element 7, [68]) and the three-dimensional two-node straight truss (Element 9, [68]) elements were applied. The following parameters for the Bodner–Partom model for description of the steel material at 20°C were taken (from Kłosowski [32]): $E = 223.0\,\text{GPa}$, $\nu = 0.3$ and $D_0 = 1 \cdot 10^4\,\text{s}^{-1}$, $Z_0 = 259.38\,\text{MPa}$, $Z_1 = 422.90\,\text{MPa}$, $Z_2 = 0.0\,\text{MPa}$, $Z_3 = 21.35\,\text{MPa}$, $n = 9.61$, $m_1 = 0.068\,\text{MPa}^{-1}$, $m_2 = 1.82\,\text{MPa}^{-1}$, $A_1 = A_2 = 0.0\,\text{s}^{-1}$, $r_1 = r_2 = 0.0$.

The graphs of the stress–strain for the strain rate $\dot{\varepsilon} = 0.01\,\text{s}^{-1}$ are given in Fig. 2. Good agreement of stress versus strain is obtained from both numerical calculations and experiment. It is worth pointing out that for different types of finite element applied in the MSC.Marc calculations the results are the same.

Additionally, Kłosowski in his work [32] presented the material parameters for the steel at 20°C for the Chaboche model. The identification of the constants for the Chaboche was based on the known parameters of the Bodner–Partom model. The following parameters for Chaboche model were established: $E = 223.0\,\text{GPa}$, $\nu = 0.3$ and $k = 210.15\,\text{MPa}$, $b = 16.74$, $R_1 = -138.48\,\text{MPa}$, $a = 611.70\,\text{GPa}$, $c = 38840.0$, $n = 9.51$, $K = 14.085\,(\text{MPa} \cdot \text{s})^{1/n}$. On the basis of these parameters the calculation for the Chaboche model was carried out (see Ambroziak [1, 2] for details). The results of this calculation are compared with the numerical analysis with the Bodner–Partom model and experiments, see Fig. 3. Both the Chaboche and Bodner–Partom models implemented to the MSC.Marc give similar results, and are comparable with experiment.

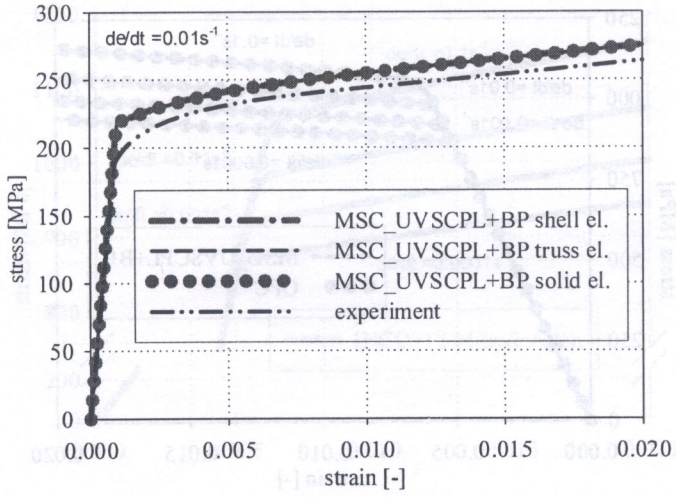

Fig. 2. Uniaxial tension test simulation for different finite element types

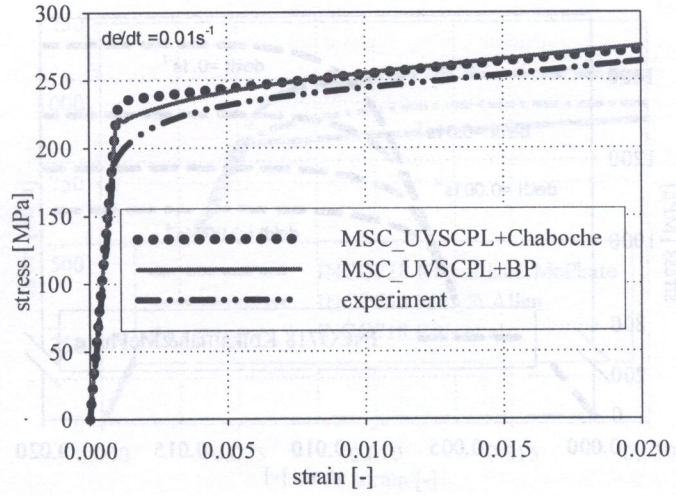

Fig. 3. Results of Chaboche and Bodner–Partom simulation of uniaxial tension test

4.3. Example 2 – INCO718 analysis

The numerical simulation of uniaxial tension tests for different strain rates using Bodner–Partom model is investigated in this example. For the finite element analysis the following material parameters were assumed (INCO718 at 650°C Milly and Allen [50], see also Kłosowski and Woznica [34]): $E = 169.0\,\text{GPa}$, $\nu = 0.3$, $D_0 = 1 \cdot 10^4\,\text{s}^{-1}$, $Z_0 = 3130.0\,\text{MPa}$, $Z_1 = 4140.0\,\text{MPa}$, $Z_2 = 2760.0\,\text{MPa}$, $Z_3 = 0.0\,\text{MPa}$, $n = 1.17$, $m_1 = 0.024\,\text{MPa}^{-1}$, $m_2 = 0.0\,\text{MPa}^{-1}$, $A_1 = A_2 = 0.0\,\text{s}^{-1}$, $r_1 = 2.86$, $r_2 = 0.0$.

The graphs of the stress versus strain for the three strain rates $\dot{\varepsilon} = 1.0 \cdot 10^{-4}$, $\dot{\varepsilon} = 1.0 \cdot 10^{-3}$, $\dot{\varepsilon} = 1.0 \cdot 10^{-2}$ and $\dot{\varepsilon} = 1.0 \cdot 10^{-1}$ are submitted in Fig. 4. In this case, besides of the MSC.Marc analysis the calculations were carried out in the own FEM code (OFC) for a simple truss inelastic analysis. Both results obtained from MSC.Marc and OFC computer programs are in good agreement.

It worth pointing out that even for the same materials in the same conditions, some material parameters are strongly different. For example, for the chosen nickel based INCO718 alloy at 650°C the numerical calculations were performed using the material parameters (see Table 3) given by: Kolkaillah and McPhate [38] (Fig. 5), Eftis *et al.* [18] (Fig. 6) and Milly and Allen [50] (Fig. 7). It is

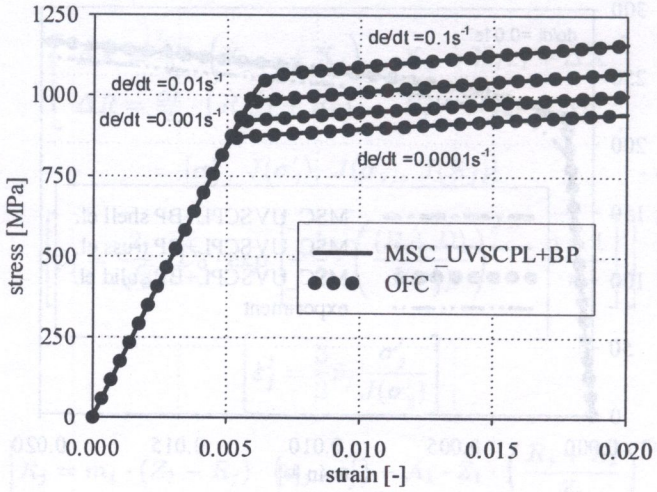

Fig. 4. Results of numerical simulations of the constant strain rates tests

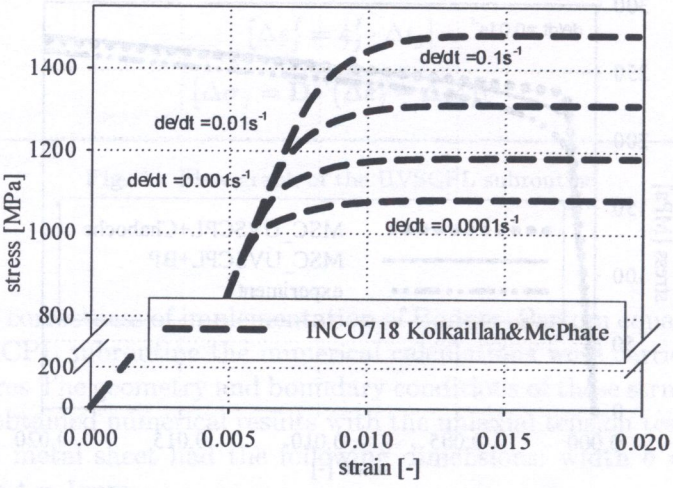

Fig. 5. Results of numerical simulations for INCO718 – parameters from [38]

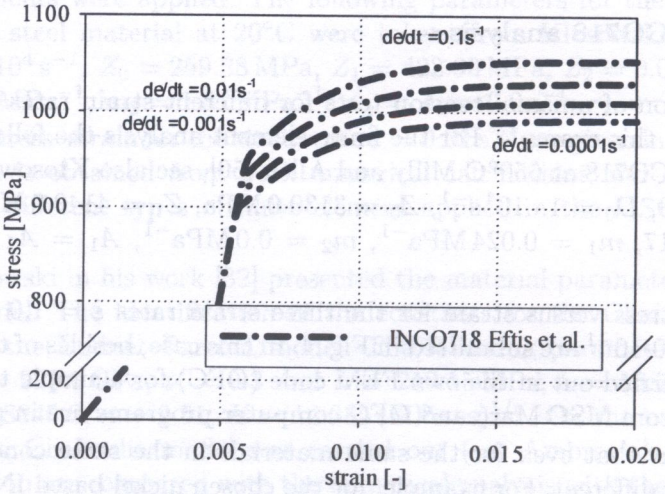

Fig. 6. Results of numerical simulations for INCO718 – parameters from [18]

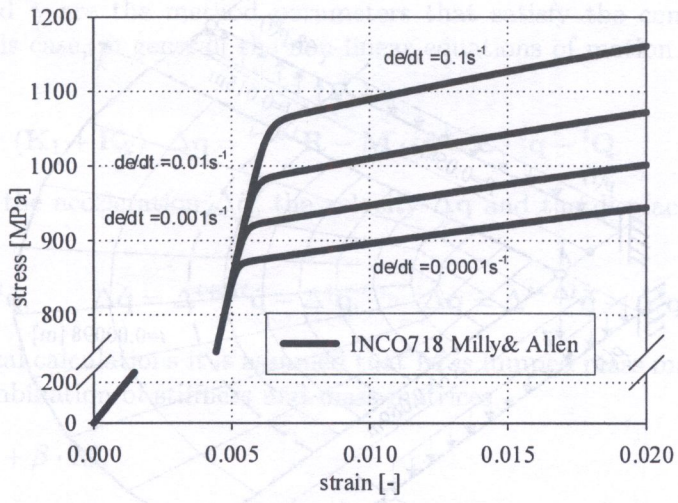

Fig. 7. Results of numerical simulations for INCO718 – parameters from [50]

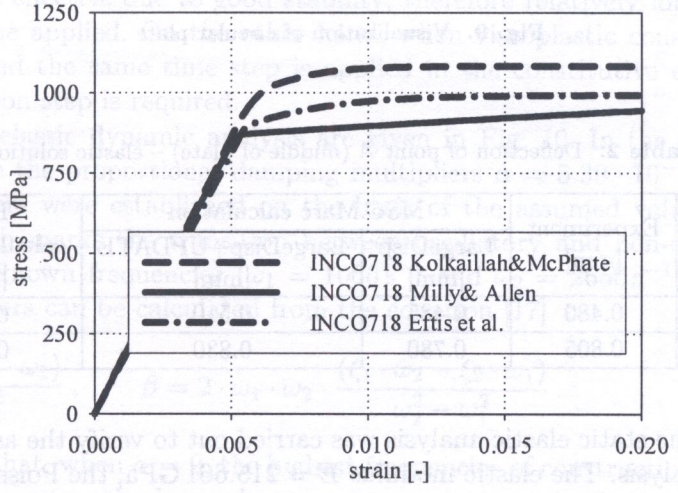

Fig. 8. Results of numerical simulations for $\dot{\varepsilon} = 1.0 \cdot 10^{-4}$

necessary to notice that even the elastic modules are different in these three investigated complete groups of material parameters.

The comparison of the numerical simulations is given in Fig. 8 for the strain rate $\dot{\varepsilon} = 1.0 \cdot 10^{-4}$. One can observe significant differences between presented material constant for the Bodner–Partom constitutive model analysis, e.g. Milly and Allen [50] observed hardening while Eftis *et al.* [18] noticed softening of the INCO718 alloy. On the other hand, Kolkaillah and McPhate [38] for the same material obtained the 20% increase of yield stress in comparison with other researches, see Fig. 8. Therefore, it is worth signalling that for the detailed investigations it is necessary to make the experiment tests and carry out the identification of the material parameters for particular cases.

4.4. Example 3 – static and dynamic steel plate analysis

The numerical analysis of circular steel plate under static and dynamic loading is studied, see Fig. 9. Due to the symmetry of the geometry and loadings only a quarter of the plate with proper symmetry boundary conditions was analysed.

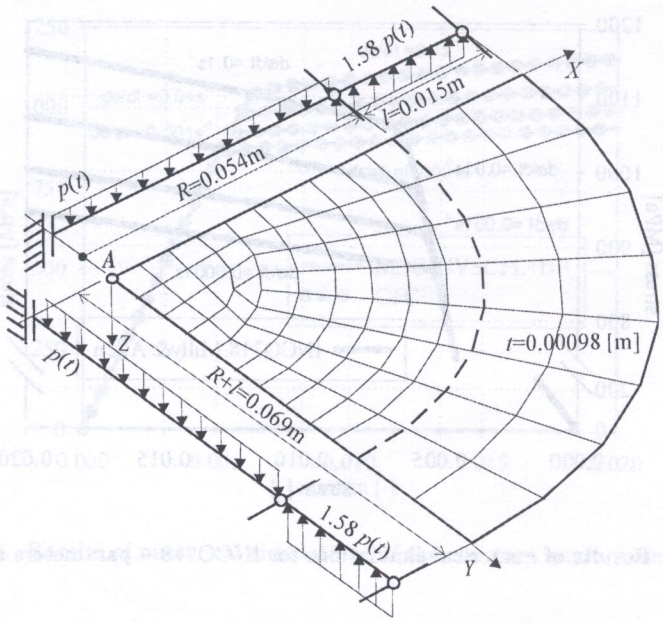

Fig. 9. Visualization of circular plate

Table 2. Deflection of point A (middle of plate) – elastic solution

Pressure [10^5 Pa]	Experiment [mm]	MSC.Marc calculation		FEM calculation [32] [mm]
		LargeDisp [mm]	LargeDisp+UPDATE [mm]	
0.5	0.480	0.485	0.510	0.430
1.0	0.805	0.780	0.830	0.715

At the beginning, the static elastic analysis was carried out to verify the assumed boundary conditions and type of analysis. The elastic modulus $E = 215.661$ GPa, the Poisson's ratio $\nu = 0.3$ and the thicknesses of plate $t = 0.00098$ m were taken. The mass density of the steel plate $\rho = 7850\,\mathrm{kg/m^3}$ was selected. In the MSC.Marc calculations two options of analysis were tested: 'LargeDisp' and 'LargeDisp+UPDATE'. With 'LargeDisp' parameter, MSC.Marc uses to the calculation the total Lagrangian method and with option 'LargeDisp+UPDATE' MSC.Marc applies to the calculation the Cauchy stresses and true strains. The results of static, elastic numerical analysis are presented in Table 2 for two chosen values of pressure. The obtained results are compared with the experiment measurements and FE calculations performed by Kłosowski [32]. A very good agreement of vertical displacements from FE calculations and experiment was obtained. These calculations confirm the assumption as to boundary conditions, values of loadings and density of mesh. For the following calculations the 'LargeDisp' option should be used. It ought to be noted that, in the work [32], Kłosowski used nine-node isoparametric shell elements. In the present numerical analysis the four-node shell elements (Element 139 [68]) were applied. The meshes are taken to correspond with numerical calculations carried out by Kłosowski [32] (the nodes are overlap in the same places).

In the first step of the dynamic analysis the elastic behaviour of the plate was investigated. The non-linear equation of motion was integrated with the Newmark algorithm [51] with the time step $\Delta t = 2.0 \cdot 10^{-5}$ s. The Newmark method is based on two principal expressions

$$
\begin{aligned}
{}^{t+\Delta t}\dot{\mathbf{q}} &= {}^{t}\dot{\mathbf{q}} + \left[(1-\delta)\cdot {}^{t}\ddot{\mathbf{q}} + \delta \cdot {}^{t+\Delta t}\ddot{\mathbf{q}}\right]\cdot \Delta t, \\
{}^{t+\Delta t}\mathbf{q} &= {}^{t}\mathbf{q} + {}^{t}\dot{\mathbf{q}}\cdot\Delta t + \left[(0.5-\gamma)\cdot {}^{t}\ddot{\mathbf{q}} + \gamma \cdot {}^{t+\Delta t}\ddot{\mathbf{q}}\right]\cdot \Delta t^2.
\end{aligned}
\tag{20}
$$

The parameters δ and γ are the method parameters that satisfy the conditions $\delta \geq 0.5$, $\gamma \geq 0.25 \cdot (0.5 + \delta)^2$. In this case, in general, the non-linear equations of motion may be written in the form

$$\mathbf{M} \cdot \Delta\ddot{\mathbf{q}} + \mathbf{C} \cdot \Delta\dot{\mathbf{q}} + (\mathbf{K}_1 + \mathbf{K}_2) \cdot \Delta\mathbf{q} = {}^{t+\Delta t}\mathbf{R} - \mathbf{M} \cdot {}^{t}\ddot{\mathbf{q}} - \mathbf{C} \cdot {}^{t}\dot{\mathbf{q}} - {}^{t}\mathbf{Q}. \tag{21}$$

The increments of the acceleration $\Delta\ddot{\mathbf{q}}$, the velocity $\Delta\dot{\mathbf{q}}$ and the displacement $\Delta\mathbf{q}$ are derived from the equations

$$\Delta\ddot{\mathbf{q}} = \Delta^{t+\Delta t}\ddot{\mathbf{q}} - \Delta^{t}\ddot{\mathbf{q}}, \qquad \Delta\dot{\mathbf{q}} = \Delta^{t+\Delta t}\dot{\mathbf{q}} - \Delta^{t}\dot{\mathbf{q}}, \qquad \Delta\mathbf{q} = \Delta^{t+\Delta t}\mathbf{q} - \Delta^{t}\mathbf{q}. \tag{22}$$

In the present numerical calculations it is assumed that $\mathbf{M}$ is lumped mass matrix, and $\mathbf{C}$ (damping matrix) is a linear combination of stiffness and mass matrices,

$$\mathbf{C} = \alpha \cdot (\mathbf{K}_1 + \mathbf{K}_2) + \beta \cdot \mathbf{M}, \tag{23}$$

where α is stiffness matrix multiplier and β is mass matrix multiplier.

Application of the Newmark method in nonlinear analysis requires iterations at each step. It is also necessary to construct and invert the stiffness matrix at each time step. Nevertheless, the Newmark algorithm is effective due to good stability; therefore relatively long integration step for elastic problems can be applied. On the other hand, when viscoplastic constitutive equations are taken into account, and the same time step is applied in the constitutive equations' integration, much smaller integration step is required.

The results of the elastic dynamic analysis are given in Fig. 10. In the analysis of the elastic vibrations of the plate the proportional damping multipliers $\alpha = 5.39 \cdot 10^{-6}$ and $\beta = 15.16$ were taken. These multipliers were established on the basis of the assumed value of critical damping $\xi_1 = \xi_2 = 0.01$ (which marks the transition between oscillatory and non-oscillatory response of a structure) and two known frequencies ($\omega_1 = 1060\,\mathrm{s}^{-1}$ and $\omega_2 = 2650\,\mathrm{s}^{-1}$, specified for $p = 1.0$ [10^5 Pa]). The multipliers can be calculated from the equation [17]

$$\alpha = 2 \cdot \frac{(\xi_2 \cdot \omega_2 - \xi_1 \cdot \omega_1)}{\omega_2^2 - \omega_1^2}, \qquad \beta = 2 \cdot \omega_1 \cdot \omega_2 \cdot \frac{(\xi_1 \cdot \omega_2 - \xi_2 \cdot \omega_1)}{\omega_2^2 - \omega_1^2}. \tag{24}$$

It should be noted that, when $\alpha = 0$, the highest frequencies of constructional system are weakly damped, while $\beta = 0$ are strongly damped.

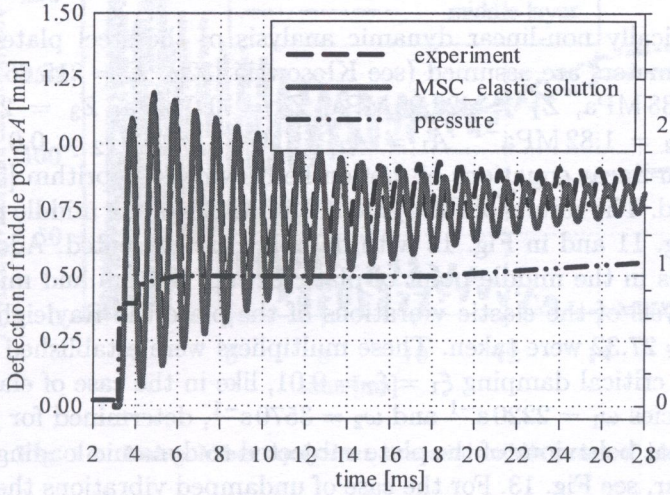

Fig. 10. Elastic vibrations of the middle point

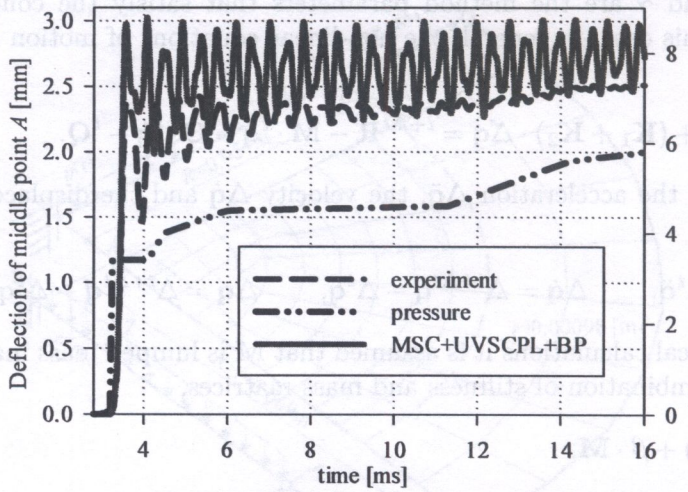

Fig. 11. Middle point of plate vibrations – analysis without damping

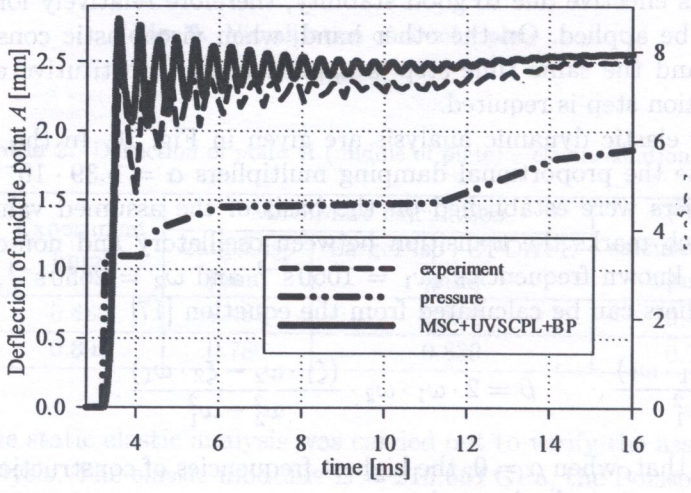

Fig. 12. Middle point of plate vibrations – analysis with damping

Finally the geometrically non-linear dynamic analysis of the steel plate was performed. The following material parameters are assumed (see Kłosowski [32]): $E = 215.661\,\text{GPa}$, $\nu = 0.3$, $D_0 = 1 \cdot 10^4\,\text{s}^{-1}$, $Z_0 = 259.38\,\text{MPa}$, $Z_1 = 422.90\,\text{MPa}$, $Z_2 = 0.0\,\text{MPa}$, $Z_3 = 21.35\,\text{MPa}$, $n = 9.61$, $m_1 = 0.068\,\text{MPa}^{-1}$, $m_2 = 1.82\,\text{MPa}^{-1}$, $A_1 = A_2 = 0.0\,\text{s}^{-1}$, $r_1 = r_2 = 0.0$. Like in the previous test to integrate the non-linear equations of motion he Newmark algorithm [51] with the time step $\Delta t = 7 \cdot 10^{-7}$ was applied. The results of the dynamic vibrations of the middle point of the steel plate without damping in Fig. 11 and in Fig. 12 with damping are presented. Additionally, the Huber–Mises equivalent stresses in the middle point of plate for top, bottom and middle layers are shown in Fig. 14. To the analysis of the elastic vibrations of the plate the Rayleigh damping multipliers $\alpha = 3.46 \cdot 10^{-6}$ and $\beta = 27.32$ were taken. These multipliers were established on the basis Eq. (24) of the assumed value of critical damping $\xi_1 = \xi_2 = 0.01$, like in the case of elastic dynamic analysis and two known frequencies $\omega_1 = 2220\,\text{s}^{-1}$ and $\omega_2 = 3570\,\text{s}^{-1}$, determined for $p = 6.1$ [10^5 Pa].

It should be noted that behaviour of the plate subjected to dynamic loading is definitely different from the static behaviour, see Fig. 13. For the case of undamped vibrations the significant difference from the experimental results is observed (Fig. 11). When the damping factor is included the solutions are very close to the results from the laboratory tests (Fig. 12). The simple damping model applied to the analysis and validity of material parameters can explain the small differences.

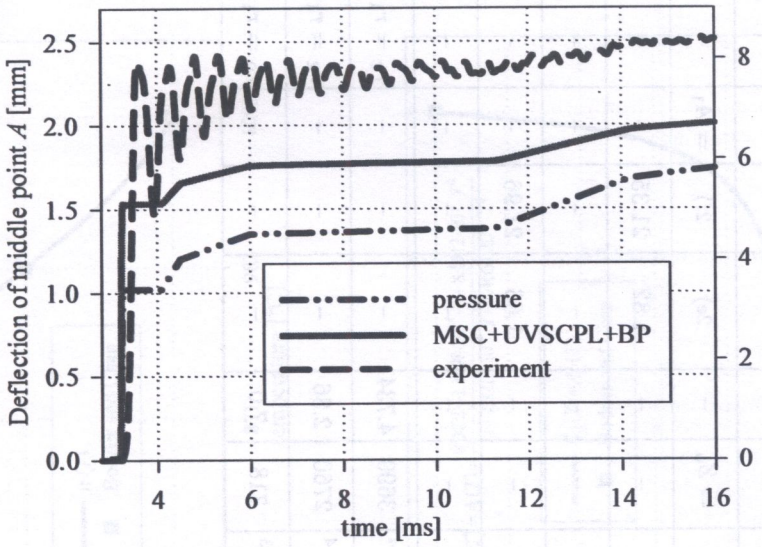

Fig. 13. Middle point deflection – inelastic static analysis

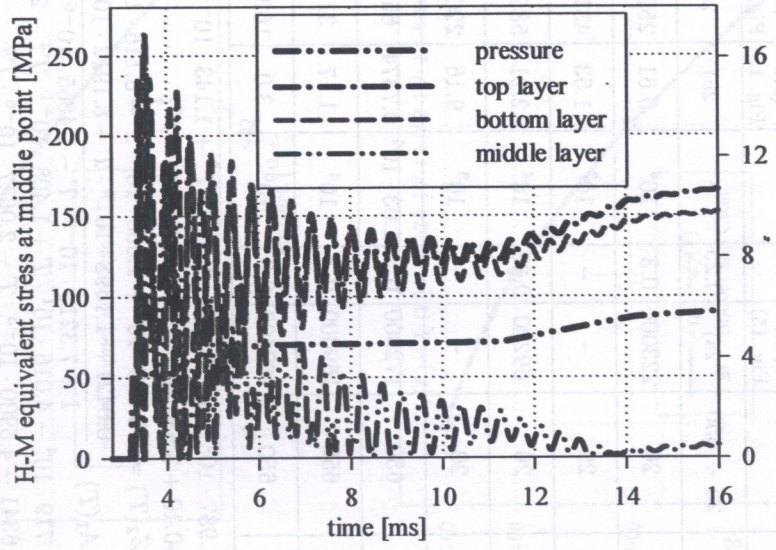

Fig. 14. Huber-Mises equivalent stress in middle point of plate

Table 3. Parameters for Bodner–Partom model for the chosen material

Material	Temp. T [°C]	E [MPa]	ν [–]	D_0 [s^{-1}]	n [–]	Z_0 [MPa]	m_1 [MPa^{-1}]	Z_1 [MPa]	A_1 [s^{-1}]	Z_2 [MPa]	r_1 [–]	m_2 [MPa^{-1}]	Z_3 [MPa]	A_2 [s^{-1}]	r_2 [–]	$\dot{p}$
B1900+Hf [10]	760 ÷ 1093	1a) (see Fig. 15)	0.3	10^4	1b) (see Fig. 15)	1c) (see Fig. 15)	0.270	3000	1d) (see Fig. 15)	$= Z_0$	2	1.52	1150	$= A_1$	2	Eq. (11)
SCS-6/Ti-15-3 [20]	25 ÷ 650	2a)	0.25	–	2b)	2c)	–	–	2d)	$= Z_0$	–	2e)	2f)	$= A_1$	–	Eq. (11)
Steel [32]	20	223000	0.3	10^4	9.61	259.38	0.068	422.90	–	–	–	1.82	21.35	–	–	Eq. (9)
Steel [64]	20	–	–	10^3	1.63	431.86	0.1214	665.94	–	–	–	–	–	–	–	Eq. (9)
Aluminium [32]	20	69200	0.33	10^4	2.21	585.32	0.34	641.87	–	–	–	1.66	21.96	–	–	Eq. (9)
Copper [64]	20	–	–	10^3	9.16	220.08	6.3872	294.12	–	–	–	–	–	–	–	Eq. (9)
INCO718 [38, 71]	650	172000	0.3	$1.03 \cdot 10^4$	0.7374	6520	0.686	7030	$6.82 \cdot 10^{-4}$	3690	4.734	–	–	–	$r_2 = r_1$	Eq. (9)
INCO718 [50, 71]	650	169000	0.3	10^4	1.17	3130	0.024	4140	$1.10 \cdot 10^{-4}$	2760	2.86	–	–	–	$r_2 = r_1$	Eq. (9)
INCO718 [18, 71]	650	162400	0.3	10^6	3.0	1621.5	0.42	1794.7	$1.50 \cdot 10^{-3}$	718	7.0	–	–	–	$r_2 = r_1$	Eq. (9)

1a) $E(T) = 1.987 \cdot 10^5 + 16.78 \cdot T - 0.1034 \cdot T^2 + 1.143 \cdot 10^{-5} \cdot T^3$;

1b) $n(T) = -0.19 + 3.58 \cdot 10^{-3} \cdot T - 2.54 \cdot 10^{-6} \cdot T^2$;

1c) $Z_0(T) = Z_2(T) = -6.186 \cdot 10^2 + 1.053 \cdot 10^1 \cdot T - 8.116 \cdot 10^{-3} \cdot T^2$;

1d) $A_1(T) = A_1(T) = \dfrac{0.0421 - 1.1698 \cdot 10^{-4} \cdot T + 8.1912 \cdot 10^{-8} \cdot T^2}{1 + 7.3215 \cdot 10^{-4} \cdot T - 1.4665 \cdot 10^{-6} \cdot T^2}$;

2a) $E(T) = 8.719 \cdot 10^4 - 4.016 \cdot 10^1 \cdot T + 1.408 \cdot 10^{-1} \cdot T^2 - 2.469 \cdot 10^{-4} \cdot T^3$;

2b) $n(T) = 4.6341 - 4.6900 \cdot 10^{-3} \cdot T - 2.0627 \cdot 10^{-6} \cdot T^2$;

2c) $Z_0(T) = Z_2(T) = 1.201 \cdot 10^3 + 5.53 \cdot 10^{-2} \cdot T - 1.435 \cdot 10^{-3} \cdot T^2$;

2d) $A_1(T{=}25) = 10^{-8}$; $A_1(T{=}315) = 4.4 \cdot 10^{-6}$; $A_1(T{=}427) = 10^{-5}$; $A_1(T{=}482) = 1$; $A_1(T{=}566) = 2.5$; $A_1(T{=}650) = 3$;

2e) $m_2(T{=}25) = 0.005$; $m_2(T{=}315) = 0.04$; $m_2(T{=}427) = 0.05$; $m_2(T{=}482) = 5$; $m_2(T{=}566) = 15$; $m_2(T{=}650) = 20$;

2f) $Z_3(T) = 3.907 \cdot 10^2 - 4.953 \cdot T + 1.40 \cdot 10^{-2} \cdot T^2$

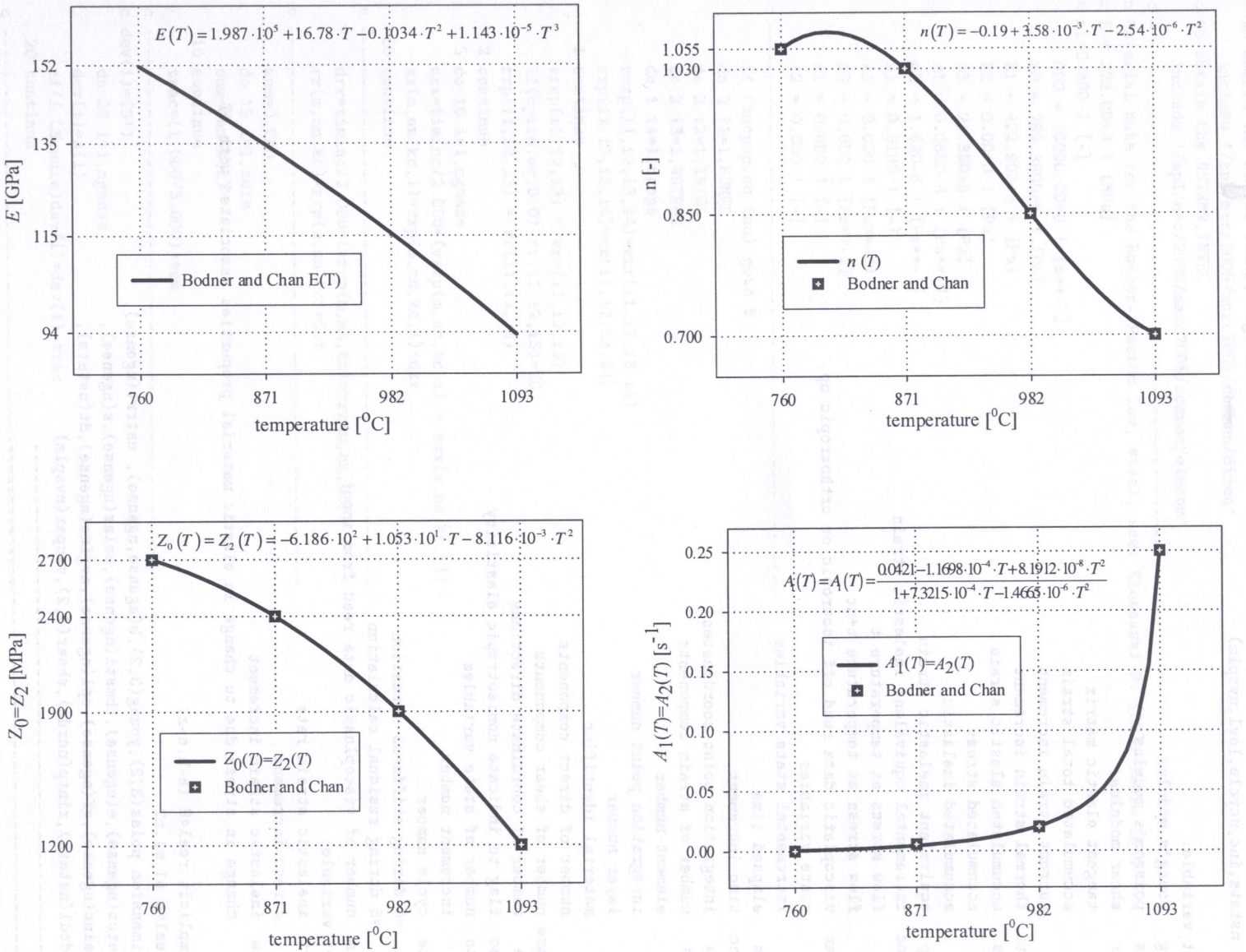

Fig. 15. Temperature dependent material parameters for B1900+Hf

Table 4. UVSCPL subroutine for Bodner–Partom model analysis

```
      subroutine uvscpl(young,poiss,shear,b,ustrrt, etot,e,thmsti,eelas,
     1 s,sinc,gf,epl,avgine,eqcrp,eqcpnc,yd,yd1,vscpar,dt,dtdl,cptim,
     2 timinc,xintp,ngense,m,nn,kc,mat,ndie,nsheare,ncrde,ianisoe,
     3 nstats,inc,ncycle,lovl,nvsplm)
c
c Input variable:
c young   young's modulus
c poiss   poisson's modulus
c shear   shear modulus
c b       tangent elastic matrix
c etot    accumulated total strain
c e       current strain increment
c thmsti  thermal strain increment
c eelas   accumulated elastic strain
c s       accumulated stress
c epl     accumulated inelastic
c eqcrp   equivalent inelastic strain
c eqcpnc  incremental equivalent inelastic strain
c yd      flow stress at temperature t
c yd1     flow stress at temperature t+dt
c vscpar  viscoplatic data read off isotropic or orthotropic op.
c dt      state variables
c dtdl    incremental state variables
c cptim   elapsed time
c timinc  time increment
c xintp   integration point coordinates
c ngens   number of strain components
c m       element number
c nn      integration point number
c kc      layer number
c mat     material identifier
c ndie    number of direct components
c nsheare number of shear components
c ncrde   number of coordinate directions
c ianiso  flag to indicate nonisotropic elasticity
c nstats  number of state variables
c inc     increment number
c ncycle  cycle number
c lovl   =4 during stiffness formation
c        =6 during residual calculation
c nvsplm  number of viscoplastic data read from input
c Output variable:
c ustrrt  inelastic strain rate
c sinc    stress increment
c avgine  inelastic strain increment
c gf      change in stress due to change in elastic material properties associated with DT
c
      implicit real*8 (a-h,o-z)
      real*8 n1,m1,m2
      dimension poiss(3,2),young(3,2),b(ngense,ngense), ustrrt(ngense),
     1 etot(ngense),e(ngense),thmsti(ngense),eelas(ngense),s(ngense),
     2 sinc(ngense),gf(ngense),epl(ngense),avgine(ngense),dt(nstats),
     3 dtdl(nstats),xintp(ncrde),shear(3,2),vscpar(nvsplm)
c -------------------------------------------------------
c -------------------------------------------------------
c Andrzej AMBROZIAK, v1 2005
c This user subroutine is used for computing the inelastic strain increment
c for an elastic-viscoplastic Bodner--Partom material.
```

```
c
      dimension xxp(100,4,10,6),xx(100,4,10,6),vxxp(100,4,10,6),
     1 vxx(100,4,10,6),vrrp(100,4,10),vrr(100,4,10),rrp(100,4,10),
     2 rr(100,4,10),dev(6),SS(6)
c to obtain the Numel, Numnp,Ndeg,Ncord
      include '/apl/msc/2005/marc2005/common/dimen'
c to obtain the NSTRM2,INTEL
      include '/apl/msc/2005/marc2005/common/elmcom'
c -------------------------------------------------------
c Material data for the Bodner--Partom law, steel, see: Klosowski P. [32], Table 16.4
c E = 223.0D+3 ! [MPa]
c ni=0.3D0 ! [-]
      DD0 = 10000.0D+0 ! [s**-1]
      Z0 = 259.380D+6 ! [Pa]
      Z1 = 422.90D+6 ! [Pa]
      Z2 = 0.0D+0 ! [Pa]
      Z3 = 21.35D+6 ! [Pa]
      m1 = 0.068D-6 ! [Pa**-1]
      m2 = 1.82D-6 ! [Pa**-1]
      n1 = 9.61D0 ! [-]
      A1 = 0.0D0 ! [Pa**-1]
      A2 = 0.0D0 ! [Pa**-1]
      r1 = 0.0D0 ! [-]
      r2 = 0.0D0 ! [-]
c -------------------------------------------------------
      if (incpop.eq.inc) goto 5
      do 2 i1=1,NUMEL
      do 2 i2=1,INTEL
      do 2 i3=1,NSTRM2
      do 1 i4=1,ngens
      vxxp(i1,i2,i3,i4)=vxx(i1,i2,i3,i4)
      xxp(i1,i2,i3,i4)=xx(i1,i2,i3,i4)
    1 continue
      vrrp(i1,i2,i3) = vrr(i1,i2,i3)
      if(cptim.eq.0.0) rr(i1,i2,i3)=Z0
      rrp(i1,i2,i3) = rr(i1,i2,i3)
    2 continue
    5 do 10 i=1,ngense
      dxx=timinc/2.0D0*(vxxp(m,nn,kc,i) + vxx(m,nn,kc,i))
      xx(m,nn,kc,i)=xxp(m,nn,kc,i)+dxx
   10 continue
c -------------------------------------------------------
      drr=timinc/2.0D0*(vrrp(m,nn,kc)+vrr(m,nn,kc))
      rr(m,nn,kc)=rrp(m,nn,kc)+drr
c -------------------------------------------------------
      sum=0.0D0
      do 15 i=1,ndie
      sum=sum+s(i)
   15 continue
      trac=(1.0D0/3.0D0)*sum
c -------------------------------------------------------
c dev(i)=(S')
      do 20 i=1,ngense
      dev(i)=s(i)
      if(i.LE.ndie)dev(i)=dev(i)-trac
   20 continue
c -------------------------------------------------------
c ddd= J(S')
      sum=0.0D0
      do 25 i=1,ngense
```

```
      sum=sum+dev(i)*dev(i)
   25 continue
      if (ndie.eq.1) sum=sum+2*trac*trac
      if (ndie.eq.2) sum=sum+trac*trac
      ddd=dsqrt(1.5*sum)
c -------------------------------------------------------
c dddS = J(S)
      sum=0.0D0
      do 30 i=1,ngense
      sum=sum+s(i)*s(i)
      if(i.gt.ndie)sum=sum+s(i)*s(i)
   30 continue
      dddS=dsqrt(1.5*sum)
c -------------------------------------------------------
c SS = S/J(S)
      do 35 i=1, ngense
      SS(i)=s(i)/dddS
      if(dddS.EQ.0.0) SS(i)=0.0D0
   35 continue
c -------------------------------------------------------
c dddXX= J(X)
      sum=0.0D0
      do 40 i=1,ngense
      sum=sum+xx(m,nn,kc,i)*xx(m,nn,kc,i)
      if(i.gt.ndie)sum=sum+xx(m,nn,kc,i)*xx(m,nn,kc,i)
   40 continue
      dddXX=dsqrt(1.5*sum)
c -------------------------------------------------------
c DP=X:(S/J(S))
      sum=0.0D0
      do 45 i=1,ngense
      sum=sum+xx(m,nn,kc,i)*ss(i)
      if(i.gt.ndie)sum=sum+xx(m,nn,kc,i)*ss(i)
   45 continue
      XSJS=sum
c -------------------------------------------------------
      if(ddd.EQ.0.0) then
      Z=0.0D0
      else
      Z = (rr(m,nn,kc)+XSJS)/ddd
      end if
c ppp - inelastic strain rate for type A of law:
      ppp=(2.0D0/dsqrt(3.0D0))*DD0*dexp((-0.5D0)*
     * ((n1+1.0D0)/n1)*Z**(2.0D0*n1))
c ppp - inelastic strain rate for type B of law
c ppp=(2.0D0/sqrt(3.0D0))*DD0*exp((-0.5D0)*Z**(2.0D0*n1))
c -------------------------------------------------------
      if(ppp.lt.1.0E-30) then
      do 50 j=1,ngense
      ustrrt(j)=0.0D0
   50 continue
      goto 950
      endif
c -------------------------------------------------------
c ustrrt - inelastic strain rate
c calculation of inelastic strain rate
      do 55 i=1,ngense
      if(ddd.EQ.0.0) then
      ustrrt(i)=0.0D0
      else
```

```
      ustrrt(i)=1.5D0*ppp*dev(i)/ddd
      endif
   55 continue
c -------------------------------------------------------
c vwp = S:dEi
      vwp=0.0D0
      sum=0.0D0
      do 60 i=1,ngens
      sum=sum+s(i)*ustrrt(i)
      if(i.gt.ndie) sum=sum+s(i)*ustrrt(i)
   60 continue
      vwp=sum
c -------------------------------------------------------
      vrr(m,nn,kc)=m1*(Z1-rr(m,nn,kc))*vwp -
     1 A1*Z1*((rr(m,nn,kc)+Z2)/Z1)**r1
      do 70 i=1,ngense
      if(dddXX.EQ.0.0) then
      ac=0.0D0
      else
      ac=xx(m,nn,kc,i)/dddXX
      end if
      vxx(m,nn,kc,i) = m2*(1.5D0*Z3*SS(i) - xx(m,nn,kc,i))*vwp
     1 - A2*Z1*1.5D0*(((2.0D0/3.0D0)*dddXX/Z1)**r2)*ac
   70 continue
c -------------------------------------------------------
c avgine - inelastic strain increment
  950 do 80 i=1,ngense
      avgine(i)=ustrrt(i)*timinc
   80 continue
c -------------------------------------------------------
      do 100 j=1,ngense
      sum=0.0D0
      do 90 i=1,ngense
      sum=sum+b(j,i)*(e(i)-avgine(i))
   90 continue
      sinc(j)=sum
  100 continue
      incpop=inc
c -------------------------------------------------------
c -------------------------------------------------------
      return
      end

c If user wants fixed stepping for creep analysis
c with DYNAMIC CHANGE in MSC then, he
c should use the following ubginc.f subroutine.
      subroutine ubginc(incf,incsubf)
      implicit real*8 (a-h,o-z)
      include '/apl/msc/2005/marc2005/common/concom'
      include '/apl/msc/2005/marc2005/common/iautcr'
c -------------------------------------------------------
      icreep=1
      icrpcn=0
      loadcn=1
c -------------------------------------------------------
      return
      end
```

5. Remarks and final conclusions

The following conclusions and remarks may be formulated:

1. In this study, the special kind of the finite element procedure for elasto-viscoplastic calculation has been developed. The obtained results confirm the stability of numerical algorithm, and the validity of the proposed procedure.

2. Due to the possibility of user's constitutive models subroutines which can be included into the MSC.Marc system, the elasto-viscoplastic Bodner–Partom constitutive equations can be directly applied in finite element analysis. It is shown how the models invented by Bodner–Partom can be applied into the open commercial code.

3. Sometimes the same material in the same conditions (for example investigated in Example 2: INCO718 alloy) demonstrate a variety of responses, which is concerned, among others, with the process of rolling or other inhomogeneities. For the particular case of investigations, the detailed identification of material parameters should be carried out.

4. The geometrically non-linear analysis of plate structures with elasto-viscoplastic physical equations for the Bodner–Partom model has been successfully carried out. Additionally, the obtained results confirm the validity of the proposed Rayleigh damping multipliers used to the calculations.

5. The proposed UVSCPL procedure for FEA is open and flexible and may be applied in various practical engineering applications.

Acknowledgements

The research was performed within Polish-French cooperation program Polonium 2005 administrated by KBN and ÉGIDE. (KBN 5598.II/2004/2005) and within Polish-German cooperation program DAAD 2004/2005 (KBN/DAAD 2004/2005 no. 09).

Calculations presented in the paper have been carried out at the Academic Computer Centre in Gdańsk (TASK).

References

[1] A. Ambroziak. Chaboche model – development and FE application. Zeszyty Naukowe Politechniki Śląskiej, **104**: 35—42, 2005.

[2] A. Ambroziak. Numerical modelling of elasto-viscoplastic Chaboche constitutive equations using MSC.Marc. *Task Quarterly*, **9**(2): 167–178, 2005.

[3] H. Anderson. An implicit formulation of the Bodner–Partom constitutive equations. *Computer and Structures*, **81**: 1405–1414, 2003.

[4] H. Andersson, C. Persson, T. Hansson. Crack growth in IN718 at high temperature. *International Journal of Fatigue*, **23**: 817–827, 2001.

[5] V.K. Arya. Efficient and accurate explicit integration algorithms with application to viscoplastic models. *International Journal for Numerical Methods in Engineering*, **39**(2): 261–279, 1996.

[6] M. Aubertin, D.E. Gill, B. Landanyi. A unified viscoplastic model for the inelastic flow of alkali halides. *Mechanics of Materials*, **11**: 63–82, 1991.

[7] R.C. Barta, L. Chen. Effect of viscoplastic relations on the instability strain, shear band initiation strain, the strain corresponding to the minimum shear band spacing, and the band width in a thermoviscoplastic material. *International Journal of Plasticity*, **17**: 1465–1489, 2001.

[8] R.C. Barta, N.A. Jaber. Failure mode transition speeds in an impact loaded prenotched plate with four thermoviscoplastic relations. *International Journal of Fracture*, **110**(1): 47–71, 2001.

[9] R.C. Batra, N.A. Jaber, M.E. Malsbury. Analysis of failure model in an impact loaded thermoviscoplastic prenotched plate. *International Journal of Plasticity*, **19**: 139–196, 2003.

[10] S.R. Bodner, K.S. Chan. Modeling of continuum damage for application in elastic-viscoplastic constitutive equations. *Engineering Fracture Mechanics,* **25**: 705–712, 1986.

[11] S.R. Bodner, Y. Partom. Constitutive equations for elastic-viscoplastic strain-hardening materials. *Journal of Applied Mechanics, ASME,* **42**: 385–389, 1975.

[12] S.R. Bodner. Review of a unified elastic-viscoplastic theory. In: K. Miller, ed., *Unified Constitutive Equations for Creep and Plasticity,* pp. 273–301. Elsevier, 1987.

[13] S.R. Bodner. *Unified Plasticity for Engineering Applications.* Kluwer Academic/Plenum Publishers, New York, 2002.

[14] J.L. Chaboche. Constitutive equations for cyclic plasticity and cyclic viscoplasticity. *International Journal of Plasticity,* **5**: 247–302, 1989.

[15] K.S. Chan, S.R. Bodner, U.S. Lindholm. Phenomenological modelling of hardening and thermal recovery in metals. *Journal of Engineering Material and Technology,* **110**: 1–8, 1988.

[16] K. Chełmiński. On the model of Bodner–Partom with nonhomogeneus boundary data. *Mathematische Nachrichten,* **214**(1): 5–23, 2000.

[17] R.W. Clough, J. Penzien. *Dynamics of Structures.* McGraw–Hill, Inc., Intl. Edition, 1993.

[18] J. Eftis, Abdel M.S. Kader, D.I. Jones. Comparisons between the modified Chaboche and Bodner–Partom viscoplastic constitutive theories at high temperature. *International Journal of Plasticity,* **6**: 1–27, 1989.

[19] I.I. Esat, H. Bahai, F.K. Shati. Finite element modelling of anisotropic elastic–viscoplastic behaviour of metals. *Finite Elements in Analysis and Design,* **32**: 279–287, 1999.

[20] M.A. Foringer, D.D. Robertson, S. Mall. A micromechanics-based approach to fatigue life modeling of titanium-matrix composites. *Composites Part B,* **28B**: 507–521, 1997.

[21] G.J. Frank, R.A. Brockman. A viscoelastic-viscoplastic constitutive model for glassy polymers. *International Journal of Solid and Structures,* **38**: 5149–5164, 2001.

[22] A.D. Freed, M.J. Virrilli. A viscoplastic theory applied to copper. *Proceedings of the MECAMAT,* Besançon, Vol. I, pp. 27–39, 1988.

[23] A.D. Freed, K.P. Walker. Refinements in viscoplastic model. In: D. Hui, T.J. Kozik, eds., *Visco-Plastic Behaviour of New Materials. The Winter Annual Meeting of the ASME,* San Francisco, 1989, pp. 10–15.

[24] P. Gwizda. On singular limits to Bodner–Partom model. *Mathematical Methods in the Applied Science,* **24**(3): 159–178, 2001.

[25] H.-P. Hackenberg. Large deformation finite element analysis with inelastic constitutive models including damage. *Computational Mechanics,* **16**(5): 315–327, 1995.

[26] T. Hart, S. Schwan, J. Lehn, F.G. Kollmann. Identification of material parameters for inelastic constitutive models: statical analysis and design of experiments. *International Journal of Plasticity,* **20**: 1403–1440, 2004.

[27] D.R. Hayhurst. Creep rapture under multi-axial state of stress. *Journal of Mechanical Physical Solids,* **20**: 381–390, 1972.

[28] L. Jiang, H. Wang, P.K. Liaw, C.R. Brooks, D.L. Klarstrom. Temperature evolution during low-cycle fatigue of ULTIMET alloy: experimental and modeling. *Mechanics of Materials,* **36**: 73–84, 2004.

[29] G.R. Johnson, W.H. Cook. A constitutive model and data for metals subjected to large strains, high strain rates and high temperatures. *7th International Symposium on Ballistics,* The Hague, pp. 541–547, 1983.

[30] A.S. Khan, S. Huang. Experimental and theoretical study of mechanical behaviour of 1100 aluminium in the strain rate range 10^{-5}–$10^{4}\,s^{-1}$. *International Journal of Plasticity,* **8**: 397–424, 1992.

[31] J. Klepaczko. The modified split Hopkinson pressure bar (in Polish). *Mechanika Teoretyczna i Stosowana,* **4**(9): 479–497, 1971.

[32] P. Kłosowski. *Non-linear Numerical Analysis and Experiments on Vibrations of Elasto-Viscoplastic Plates and Shells* (in Polish). Politechnika Gdańska, Gdańsk 1999.

[33] P. Kłosowski, D. Weichert, K. Woznica. Dynamic of elasto-viscoplastic plates and shells. *Archives of Applied Mechanics,* **65**(5): 326–345, 1995.

[34] P. Kłosowski, K. Woznica. Comparative analysis of dynamic behaviour of an elasto-viscoplastic truss element. *Machine Dynamics Problems,* **24**(3): 33–53, 2000.

[35] P. Kłosowski, K. Woznica. Numerical treatment of elasto viscoplastic shells in the range of moderate and large rotations. *Computational Mechanics,* **34**: 194–212, 2004.

[36] P. Kłosowski, K. Woznica, D. Weichert. Comparison of numerical modelling and experiments for the dynamic response of circular elasto-viscoplastic plates. *European Journal of Mechanics A/Solids,* **19**: 343–359, 2000.

[37] P. Kłosowski, A. Zagubień, K. Woznica. Investigation on rheological properties of technical fabric Panama. *Archives of Applied Mechanics,* **73**(9-10): 661–681, 2004.

[38] F.A. Kolkaillah, A.J. McPhate. Numerical representation of Bodner viscoplastic constitutive model. *Journal of Engineering Mechanics, ASCE,* **10**: 195–223, 1989.

[39] M.A. Korhonen, S.P. Hannjula, C.Y. Li. *State variable theories based on Hart's formulation.* In: K. Miller, ed., *Unified Constitutive Equations for Creep and Plasticity,* pp. 89–138. Elsevier, 1987.

[40] E. Krempl, J.J. McMahon, D. Yao. Viscoplasticity based on overstress with a differential growth law for the equilibrium stress. *Mechanics of Materials,* **5**: 35–48, 1984.

[41] R.D. Krieg, J.C. Swearengen, W.B. Jones. A physically based internal variable model for rate dependent plasticity. In: K. Miller, ed., *Unified Constitutive Equations for Creep and Plasticity*, pp. 245–271. Elsevier, 1987.

[42] J.L. Kroupa, M. Bartsch. Influence of viscoplasticity on the residual stress and strength of titanium matrix composite. *Composites Part B*, **29B**: 633–642, 1998.

[43] T. Lehmann. *General Frame for Definition of Constitutive Laws for Large Non-Isothermic Elastic-Plastic and Elastic-Viscoplastic Deformations.* Courses and Lectures, Vol. **281**, Springer, Wien/New York, 1984.

[44] A. Leonov. Nonequilibrum thermodynamics and rheology of viscoelastic polymer media. *Rheol. Acta*, **15**: 85–98, 1976.

[45] R. Liang, A.S. Khan. An critical review of experimental results and constitutive models for BCC and FCC metals over a wide range of strain rates and temperatures. *International Journal of Plasticity*, **15**: 963–980, 1999.

[46] C.J. Lissenden, C.T. Herakovich. Numerical modelling of damage development and viscoplasticity in metal matrix composites. *Computer Methods in Applied Mechanics and Engineering*, **126**: 289–303, 1995.

[47] R. Mahnken, E. Stein. Parameter identification for viscoplastic models based on analytical derivation of a least-squares functional and stability investigations. *International Journal of Plasticity*, **12**(4): 451–479, 1996.

[48] A. Miller. *An inelastic constitutive model for monotonic, cyclic and creep deformation (Part I and II). Journal of Engineering Material and Technologies, ASME*, **98**: 97–105 and 106–113, 1976.

[49] A.K. Miller, ed. *Unified Constitutive Equations for Creep and Plasticity.* Elsevier Applied Science, London 1987.

[50] T.M. Milly, D.H. Allen. A comparative study of non-linear rate-dependent mechanical constitutive theories for crystalline solids at elevated temperatures. *Technical Report API-E-5-82,* Virginia Polytechnic Inst. and State University, Blacksburg, 1982.

[51] N.M. Newmark. A method of computation for structural dynamics. *Journal of the Engineering Mechanics Division*, **85**: 67–94, 1959.

[52] P. Perzyna. Fundamental problems in viscoplasticity. *Advanced in Mechanics*, **9**: 243–377, 1966.

[53] P. Perzyna. *Thermodynamics of Elastic Materials* (in Polish). PWN, Warszawa, 1978.

[54] M.B. Rubin. A time integration procedure for plastic deformation in elastic-viscoplastic metals. *Zeitschrift für Angewandte Mathematik und Physik (ZAMP)*, **40**(6): 846–871, 1989.

[55] M.B. Rubin, S.R. Bodner. An incremental elastic-viscoplastic theory indicating a reduced modulus for non-proportional buckling. *International Journal of Solid and Structures*, **32**(20): 2967–2987, 1995.

[56] C. Sansour, F.G. Kollmann. Large viscoplastic deformations of shells. Theory and finite formulation. *Computational Mechanics*, **21**(6): 512–525, 1998.

[57] C. Sansour, F.G. Kollmann. On theory and numerics of large viscoplastic deformation. *Computer Methods in Applied Mechanics and Engineering*, **146**: 351–351, 1997.

[58] C. Sansour, W. Wagner. A model of finite strain viscoplasticity based on unified constitutive equations. Theoretical and computational considerations with applications to shell. *Computer Methods in Applied Mechanics and Engineering*, **191**: 423–450, 2001.

[59] C. Sansour, W. Wagner. Viscoplasticity based on additive decomposition of logarithmic strain and unified constitutive equations. Theoretical and computational considerations with reference to shell applications. *Composite Structures*, **81**: 1583–1594, 2003.

[60] F.K. Shati, I.I. Esat, H. Bahai. FEA modelling of visco-plastic behaviour of metal matrix composites. *Finite Elements in Analysis and Design*, **37**: 263–272, 2001.

[61] A.F. Skipor, S.V. Harren. Thermal cycling of temperature and strain rate dependent solder joints. *Mechanics of Time-Dependent Materials*, **2**: 59–83, 1998.

[62] S.-Ch. Song, Z.-P. Duan, D.-W. Tan. The application of B-P constitutive equations in the finite element analysis of high velocity impact. *International Journal of Solid and Structures*, **38**: 5215–5222, 2001.

[63] E.A. Steck. A stochastic model for the high-temperature plasticity of metals. *International Journal of Plasticity*, **1**: 243–258, 1985.

[64] M. Stoffel. *Nichtlineare Dynamic von Platten.* der Rheinisch-Westfälischen Technischen Hochschule Aachen, Aachen, 2000.

[65] M. Stoffel. Sensitivity of simulations depending on material parameter variations. *Mechanics Research Communications*, **32**: 332–336, 2005.

[66] J.C. Sung, J.D. Achenbach. Heating at a propagating crack tip in a viscoplastic material. *International Journal of Fracture*, **44**(4): 301–309, 1990.

[67] S. Tanimura. A practical constitutive equation covering a wide range of strain rates. *Journal of International Engineering Science*, **17**: 997–1004, 1979.

[68] Users handbook: *MSC.MARC Volume B: Element library, Version 2003.* MSC.Software Corporation 2003.

[69] Users handbook: *MSC.MARC Volume D: User subroutines and special routines, Version 2003.* MSC.Software Corporation 2003.

[70] M.A.H. van der Aa, P.J.G. Schreurs, F.P.T. Baaijens. Modelling of the wall ironing process of polymer coated sheet metal. *Mechanics of Materials*, **33**: 555–572, 2001.

[71] K. Woznica. *Dynamique des Structures Elasto-Viscoplastique.* Cahiers de Mechanique, Lille, 1998.

[72] K. Woznica, P. Kłosowski. Evaluation of viscoplastic parameters and its application for dynamic behaviour of plates. *Archives of Applied Mechanics*, **70**(8-9): 561–570, 2000.

[73] Q.-S. Yang, Q.-H. Qin. Fiber interactions and effective elasto-plastic properties of short-fiber composites. *Composite Structures*, **54**: 523–528, 2001.

[74] F. Zaïri, M. Naït-Abdelaziz, K. Woznica, J.-M. Gloaguen. Constitutive equations for the viscoplastic-damage behaviour of a rubber-modified polymer. *European Journal of Mechanics A/Solids*, **24**: 169–182, 2005.

[75] F. Zaïri, K. Woznica, M. Naït-Abdelaziz. Phenomenological nonlinear modelling of glassy polymers. *Comptes Rendus Mecanique*, **333**: 359–364, 2005.

[76] F.J. Zerilli, R.W. Armstrong. Dislocation-mechanics-based constitutive relations for material dynamics calculations. *Journal of Applied Physics*, **61**(5): 1816–1825, 1987.

[77] Ch. Zhang, I.D. Moore. Nonlinear mechanical response of high density Polyethylene. Part II: Uniaxial constitutive modeling. *Polymer Engineering and Science*, **37**(2): 414–420, 1997.

[78] Ya.A. Zhuk, I.K. Senchenkov, V.I. Kozlov, G.A. Tabieva. Axisymmetric dynamic problem of coupled thermoplasticity. *International Applied Mechanics*, **37**(10): 1311–1317, 2001.